SiB4 Version 2 Quality and Uncertainty Assessment

Katherine Haynes, Ian Baker, and Scott Denning
Department of Atmospheric Science
Colorado State University
Fort Collins, Colorado, USA
katherine.haynes@colostate.edu

***Abstract*—To assess the quality and uncertainty of the Simple Biosphere Model (SiB4) version 2 output, we have evaluated model predictions against site observations and satellite data. Comparing modeled fluxes against tower eddy covariance data from 143 sites shows that SiB4 predicts the vegetation phenology well, with land-atmosphere exchanges of carbon and energy that are within the ranges seen by the towers for nearly all plant functional types. Although SiB4 underestimates the carbon drawdown at specific forest sites due to being initialized with mature, steady-state carbon pools, globally SiB4 matches the annual global gross primary production (GPP) from both upscaling flux data and satellite data within 8%. Comparing multi-year boreal summertime (JJA) mean leaf area index (LAI) predicted by SiB4 to MODIS reveals similar patterns of vegetation coverage and spatial gradients; however, SiB4 tends to overestimate the LAI in tropical forests and underestimate the LAI in temperate and boreal forests. Site-specific LAI pulled out of the MODIS dataset confirm this finding for tropical EBF, but site comparisons at 45 DBF, ENF, and MXF sites show SiB4 has a higher LAI than MODIS. Similar to the flux data, seasonal patterns of LAI match between the model predictions and satellite observations, further supporting the SiB4 predictive phenology methodology. Finally, SiB4 predicted biomass is compared against remotely sensed carbon biomass in the tropics. Similar to the LAI pattern, SiB4 is able to simulate the gradient of biomass from forests down to grasslands; however, it overestimates the biomass of mature tropical forests.**

I. Carbon and Energy Fluxes

We have compared SiB4 carbon and energy fluxes to eddy covariance and satellite data.

A. Site Comparisons

We evaluated SiB4 land-atmosphere exchanges of carbon and energy against fluxes at 143 tower sites in the Fluxnet network over the time period from 1998 to 2015. All site Fluxnet IDs and DOIs are listed in Table I by plant functional type (PFT). Of all sites, 133 came from the FLUXNET2015 dataset (Pastorello et al. [2020]) and are used here following the terms of the CC-BY-4.0 data usage license. The remaining 10 sites came from the European Fluxes Database Cluster following their open data use policy.

At each site, we comparted the monthly mean flux data against the simulated SiB4 flux in the grid cell containing the tower, using the results for the PFT that matches the observations. For sites with mixed vegetation coverage, we combined the simulated PFTs using vegetation coverage fractions from the site descriptions and documentation. We have grouped results for each individual PFT by vegetation type (forests, grasslands, shrubs, and crops).

1) Net Ecosystem Exchange: Net ecosystem exchange (NEE) for all the PFTs are shown in Figures 1, 2, and 3. The mean observed flux across all sites with the indicated PFT is shown in the solid black line and the mean SiB4 simulated flux is shown in the solid red line. The gray bars indicate the range range of Fluxnet fluxes per month, and the red dashed lines indicate the range of SiB4 fluxes per month.

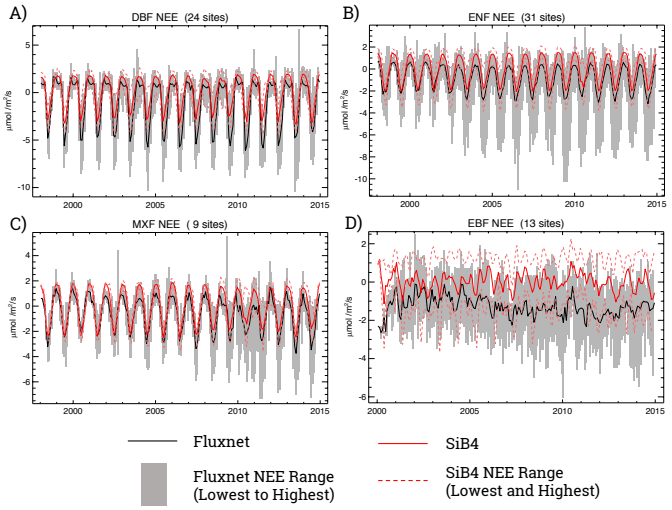

Fig. 1. FLUXNET2015 (black) and SiB4 (red) monthly mean NEE at forest sites. A) Deciduous Broadleaf Forest (DBF), B) Evergreen Needleleaf Forest (ENF), C) Mixed Forests (MXF), and D) Evergreen Broadleaf Forest (EBF).

Mean NEE from 77 forest sites is shown in Figure 1. Since deciduous broadleaf forest (DBF), evergreen needleleaf forest (ENF), and mixed forests (MXF) are prevalent in temperate climates, the mean NEE across these sites has a strong seasonal cycle, as seen in Figure 1A-C. SiB4 simulates the timing of the mean seasonality seen across the sites; however, it underestimates the magnitude of the summer drawdown and overestimates the respiration. This is because SiB4 was initialized with carbon pools representative of mature forests, yet many of the forest sites in the Fluxnet system are in the growth phase of succession and are sinks of carbon. This is particularly evident for DBF, where the time-mean NEE over the 15 years of data across all sites is < 0, indicating these sites are strong sinks. In contrast, the time-mean NEE for SiB4 is

$\sim$0, which is expected since SiB4 was initialized with steady-state carbon pools of mature forests. Despite underestimating the mean seasonal sink of carbon across the forest sites, the simulated fluxes are able to capture the phenology, and the fluxes lie within the ranges seen in the observations.

The mean NEE for broadleaf evergreen forest (EBF) sites is shown in Figure 1D. The mean observed flux across all towers shows that these sites are sinks of carbon; however, since SiB4 was initialized for mature forests it has balanced fluxes, with NEE at the top of the range seen in Fluxnet data. Despite this offset, SiB4 captures the seasonal patterns seen across the sites reasonably well. For example, SiB4 and eddy covariance data both show that the sites are sinks of carbon at the beginning of 2010, yet by mid-year both show reduced uptake by nearly the same amount of $\sim 2\,\mu\mathrm{mol\,m^{-2}\,s^{-1}}$. This seasonal pattern can be seen both in the observations and the predictions throughout the 15-year record; however, compared to the observations SiB4 overestimates the transition from source to sink the last two years.

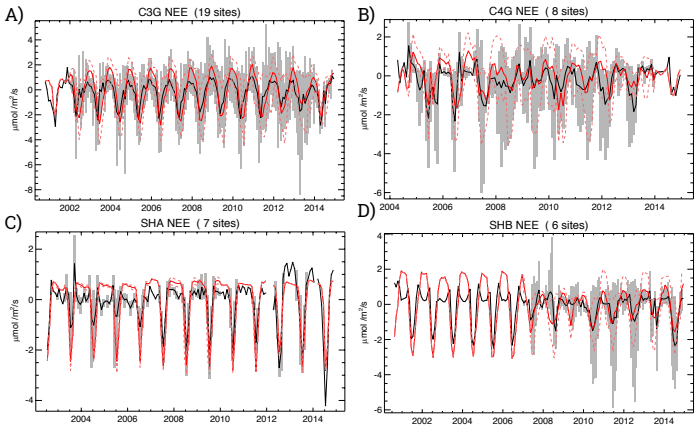

Fig. 2. FLUXNET2015 (black) and SiB4 (red) monthly mean NEE at grassland (top) and shrub (bottom) sites . A) C3 non-arctic grassland (C3G), B) C4 grassland (C4G), C) arctic shrubs (SHA), and D) non-arctic shrubs (SHB).

Grassland NEE is shown in Figure 2 (top). At C3 grassland sites (Figure 2A), SiB4 and Fluxnet sites show similar seasonal timing and drawdown magnitudes (within $0.2\,\mu\mathrm{mol\,m^{-2}\,s^{-1}}$). Overall, SiB4 predicts the phenology well, particularly the timing of the start of the growing season, but it tends to delay the end of the growing season by a month some of the years. While the range of NEE across sites is not as large in SiB4 as in the observations (gray boxes versus red dashed lines), the predicted fluxes are well within the observed NEE range. The C4 grasslands included in FLUXNET15 are predominantly desert sites, as indicated by the relatively small NEE seen in both the observations and in SiB4. Rather than having a clear seasonal cycle, the vegetation at these sites responds to rain and weather events, and this behavior is well-captured by the SiB4 overall. The flux magnitude is also similar between the observations and model, matching within $0.5\,\mu\mathrm{mol\,m^{-2}\,s^{-1}}$ for every month. For grasslands, overall the dominant phenological events and flux magnitudes are predicted within the observed site spread.

NEE at shrub sites is shown in Figure 2 (bottom). Arctic shrubs (Figure 2C) are characterized by short growing seasons, which is seen in the observations and predicted by SiB4. Compared to the arctic sites, the non-arctic shrub sites (Figure 2D) have a similar mean seasonal cycle amplitude. Timing between Fluxnet and SiB4 matches well, as the mean carbon flux remains within $0.6\,\mu\mathrm{mol\,m^{-2}\,s^{-1}}$ for all sites across the entire time period.

Lastly, NEE at crop sites is shown in Figure 3. Although limited crop-specific sites are included in the FLUXNET2015 dataset, the available sites illustrate that SiB4 predicts the short and intense growing season characterized by maize (MZE), soybeans (SOY), and winter wheat (WWT). The SiB4 predictions at generic crop sites is not as good as at specific crop locations due to the mismatch between the general crop methodology and the specific crops being observed in the tower data; however, SiB4 is able to predict the mean flux magnitude and timing within the range seen in the observations. For some years the mean NEE differences are within 0.1 $\mu\mathrm{mol\,m^{-2}\,s^{-1}}$, while other years differences up to $3\,\mu\mathrm{mol\,m^{-2}\,s^{-1}}$ occur during the peak growing season, highlighting the importance of interannual variability as well as specific crop type planted each year.

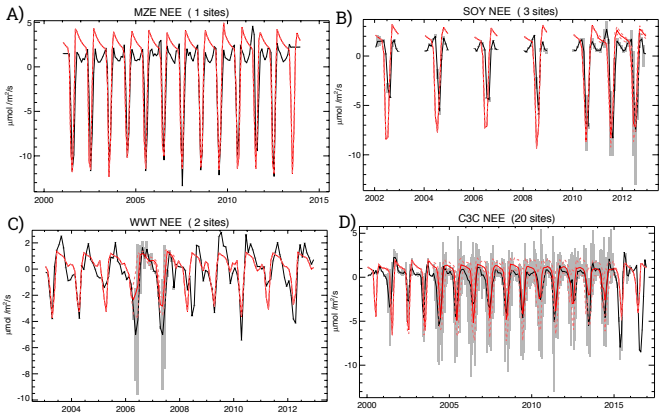

Fig. 3. FLUXNET2015 (black) and SiB4 (red) monthly mean NEE at crop sites. A) Maize (MZE), B) Soybean (SOY), C) Winter Wheat (WWT), and D) Generic C3 Crops (C3C).

2) Gross Primary Productivity: Select sites have partitioned NEE into gross primary production (GPP) and ecosystem respiration (RESP), and we have evaluated SiB4 against these carbon flux components. The FLUXNET15 dataset includes a variety of different methods for flux partitioning. Although these different methods impact the relative flux component magnitudes, for simplicity across sites we used the fluxes calculated using the reference nighttime variable ustar threshold (NT_VUT_REF; Papale et al. [2006] and Barr et al. [2013]). If there were values below zero, we instead used the results from the daytime partitioning method (DT_VUT_MEAN; Lasslop et al. [2010]) to prevent unrealistic errors or compensating

biases. GPP for forest, grassland, shrub, and crop sites are shown in Figures 4-6.

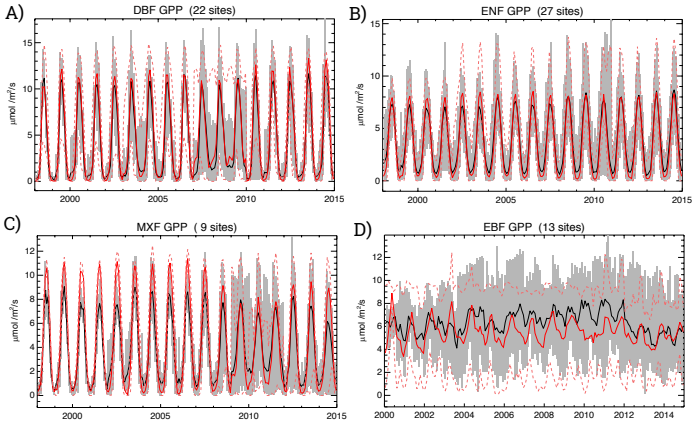

Fig. 4. FLUXNET2015 (black) and SiB4 (red) monthly mean GPP at forest sites. A) Deciduous Broadleaf Forest (DBF), B) Evergreen Needleleaf Forest (ENF), C) Mixed Forests (MXF), and D) Evergreen Broadleaf Forest (EBF).

Looking at forest PFTs, SiB4 predicts both the mean seasonality and magnitude of GPP for DBF and ENF remarkably well (Figure 4A and B), matching the observations within 0.5 μmol m^{-2} s^{-1} ($\sim$5%). In addition, SiB4 predicts a similar range and seasonal cycle between sites as seen in the FLUXNET2015 dataset, with a mean seasonal maximum GPP across sites of $\sim$14 over the time period. Mixed forest GPP (Figure 4C) tends to be overestimated by SiB4 during the peak growing season compared to the observations, in some cases by $>$30%. We suspect this is due to incorrect partitioning between DBF and ENF, yet despite this, the predicted GPP remains close to the upper end of the range seen in observations and the timing of the seasonal cycle matches remarkabely well over the 17-year time period.

The EBF GPP is shown in Figure 4D. SiB4 systematically underestimates the GPP compared to the FLUXNET2015 sites by $\sim$1.5 μmol m^{-2} s^{-1} from 2005 to 2012. Despite differences in the mean values, the monthly variability is similar to the observations throughout the entire time period.

Grassland GPP is shown in Figure 5 (top). At non-arctic C3 grassland sites (Figure 5A), SiB4 simulates the mean timing of both the start and end of season in the same month as in the observations and is able to predict interannual variability, as evidenced by the reduced uptake during 2013. SiB4 has a tendency to overestimate the mean peak summertime uptake by $\sim$10-12%, but it matches the range of GPP across sites. Predicted and observed GPP match for C4 grasslands as well (Figure 5B). SiB4 predicts the timing of increased GPP well, including capturing secondary peaks that occur at the end of growing seasons. From 2007-2011 SiB4 predicts the amplitude of the mean seasonal cycle within 1 μmol m^{-2} s^{-1} ($\sim$12%).

Shrub GPP is shown in Figure 5 (bottom). Artic sites have a short growing season with peak GPP of $\sim$3.6 in both FLUXNET2015 and SiB4, while non-arctic sites have less-defined phenology with a lower mean and higher variability

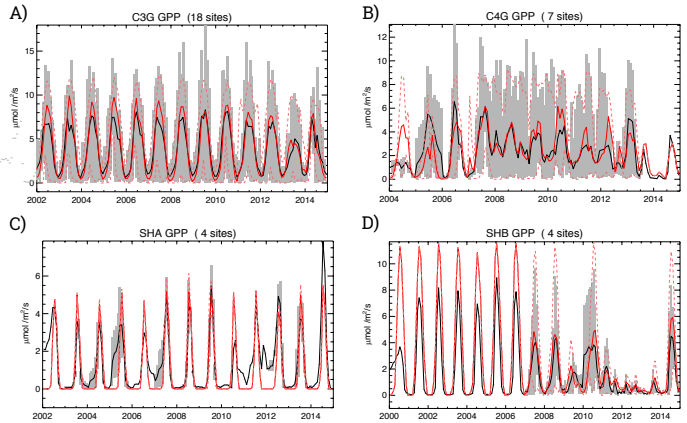

Fig. 5. FLUXNET2015 (black) and SiB4 (red) monthly mean GPP at grassland (top) and shrub (bottom) sites. A) C3 non-arctic grassland (C3G), B) C4 grassland (C4G), C) arctic shrub (SHA), and D) non-arctic shrub (SHB).

across sites. While SiB4 overestimates the GPP for the single site available between 2000-2006, once additional sites are included SiB4 matches the mean within 0.5 μmol m^{-2} s^{-1} and the across-site range within 2 μmol m^{-2} s^{-1} for the remainder of the time period.

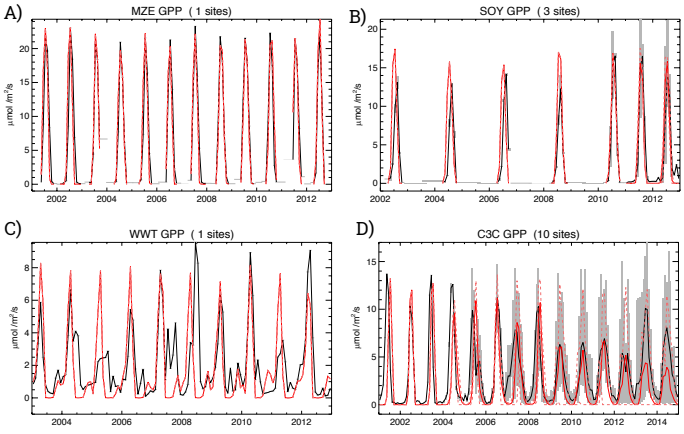

Fig. 6. FLUXNET2015 (black) and SiB4 (red) monthly mean GPP at crop sites. A) Maize (MZE), B) Soybean (SOY), C) Winter Wheat (WWT), and D) Generic C3 Crops (C3C).

Finally, crop GPP is shown in Figure 6. Although only a handful of sites are available for comparison, SiB4 again matches the timing and magnitude of uptake well, especially for MZE, SOY, and half of the years for WWT and C3C. The planting date for crops is predicted well, and the only year with substantial differences in the start of the growing season is 2008 for WWT, where SiB4 predicts crop growth earlier by a month. The end of season mismatches for WWT result from the harvest differences, where in the model harvest results in the rapid drop in GPP by SiB4. Overall the SiB4 predicts the main crop GPP fluxes well.

3) Ecosystem Respiration: Ecosystem respiration (RESP) is shown in Figures 7-9. For DBF and MXF, SiB4 overestimates

the respiration, with carbon release rates nearly double that of observed in some years. Since SiB4 uses steady-state carbon pools, the mismatch in respiration is likely due to this initialization and lack of pool adjustment to capture ecological succession. Although high, the mean SiB4 respiration still falls within the observed range. The predicted respiration at ENF forest sites more closely matches the observations, particularly from 2008-2015. Prior to 2008, the simulated overestimate is between 0.2-0.5 μmol m^{-2} s^{-1}, while from 2008 onwards the differences between SiB4 and Fluxnet are $<$0.2 μmol m^{-2} s^{-1}. The maximum respiration rates seen across the sites are also similar between predicted and observed.

For EBF (Figure 7D), the mean observed and predicted RESP over the time period is nearly identical at 5.7 μmol m^{-2} s^{-1}. Additionally, lower respiration rates for 2012 and 2013 appear in both FLUXNET2015 and SiB4, and the minimum and maximum respiration rates across the sites are similar until 2010, when SiB4 starts seen reduced respiration across all tropical forest sites. SiB4 shows less accuracy in predicting the timing of monthly RESP variability, with differences up to 18%.

Grassland respiration is shown in Figure 8 (top). For C3 grasslands, the predicted minimum and mean respiration rates match the observations well, but the maximum rates are underestimated by $>$5 μmol m^{-2} s^{-1} from 2009-2011. At C4 sites, SiB4 more closely matches the maximum respiration rates; however, differences of $>$1 μmol m^{-2} s^{-1} occur in the mean RESP during specific months.

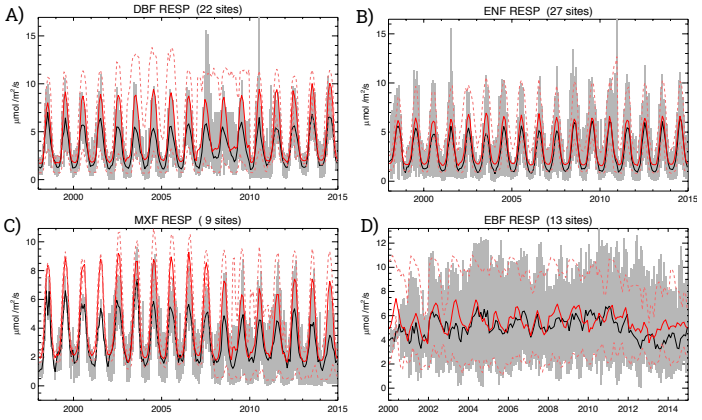

Fig. 7. FLUXNET2015 (black) and SiB4 (red) monthly mean RESP at forest sites. A) Deciduous Broadleaf Forest (DBF), B) Evergreen Needleleaf Forest (ENF), C) Mixed Forests (MXF), and D) Evergreen Broadleaf Forest (EBF).

Ecosystem respiration for shrubs is shown in Figure 8 (bottom). For both arctic and non-arctic shrubs, the modeled RESP matches the behavior seen in the observations. For SHA, SiB4 predicts the short season, mean rate, and maximum rate. For SHB, once more than one site provides data beginning in 2007, SiB4 predicts the respiration well, including capturing the downward trend from 2010-2014. At all sites, SiB4 tends to overestimate the respiration in the winter. Although model overstimation is certainly a possibility, another possibility is an underestimation in the observations due to higher eddy

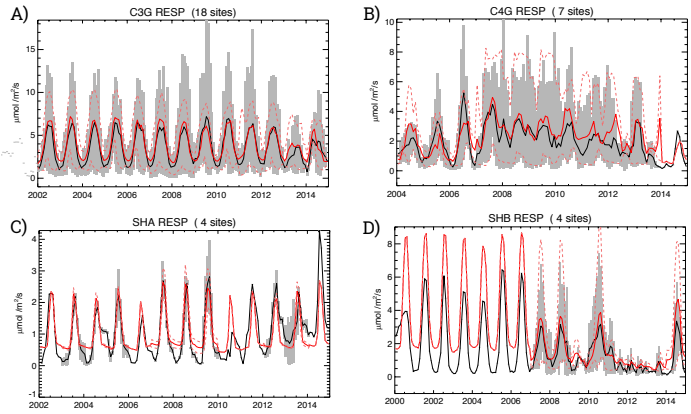

Fig. 8. FLUXNET2015 (black) and SiB4 (red) monthly mean RESP at grassland (top) and shrub (bottom) sites. A) C3 non-arctic grassland (C3G), B) C4 grassland (C4G), C) arctic shrub (SHA), and D) non-arctic shrub (SHB).

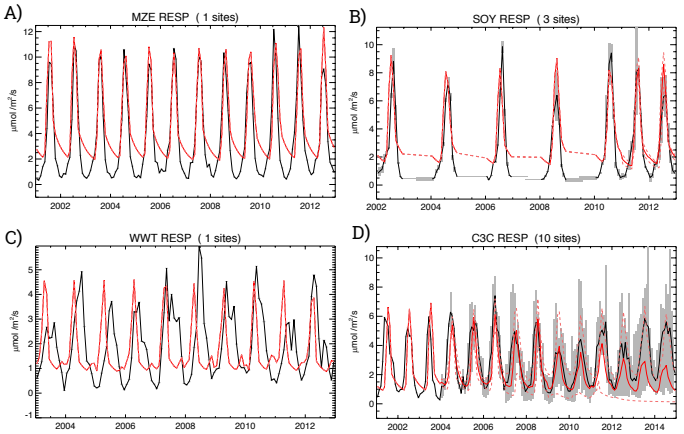

Fig. 9. FLUXNET2015 (black) and SiB4 (red) monthly mean RESP at crop sites. A) Maize (MZE), B) Soybean (SOY), C) Winter Wheat (WWT), and D) Generic C3 Crops (C3C).

covariance uncertainties associated with colder, more stratified atmospheric conditions, especially since recent work suggests that tundra soils remain active during the winter (e.g. Commane et al. [2017]).

Crop RESP is shown in Figure 9. The features seen for RESP are similar to GPP: short growing seasons with rapid increases and decreases in RESP. The predominant difference between observed and predicted crop respiration is the early peak in respiration modeled by SiB4, which is typically 1-2 months prior to the observed maximum respiration. Additionally, SiB4 overestimates the winter respiration; however, this is due to the treatment of crops in the model. At harvest in SiB4, most of the carbon is deposited in the soil carbon pools and left to decay to constrain the carbon cycle. At these sites, it is likely that more of the carbon is removed by farmers, lowering the amount of carbon available during the winter for respiration.

4) Latent Heat Flux: Land-atmosphere latent heat fluxes (LH) are shown in Figures 10-12. For forests, similar to the carbon fluxes, SiB4 predicts the timing of the seasonal cycle matching the observations. For DBF and MXF, SiB4 overestimates the peak summer flux by up to 20 $W\,m^{-2}$ (25%); however, in most cases the predicted LH is within the range seen at the sites in FLUXNET2015. For tropical forests, the SiB4 minimum, mean, and maximum latent heat fluxes remains within 10 $W\,m^{-2}$ until 2010, when larger differences (up to 20 $W\,m^{-2}$) occur as the observations trend downwards during this time period, while SiB4 only has seasonlly decreasing latent heat fluxes.

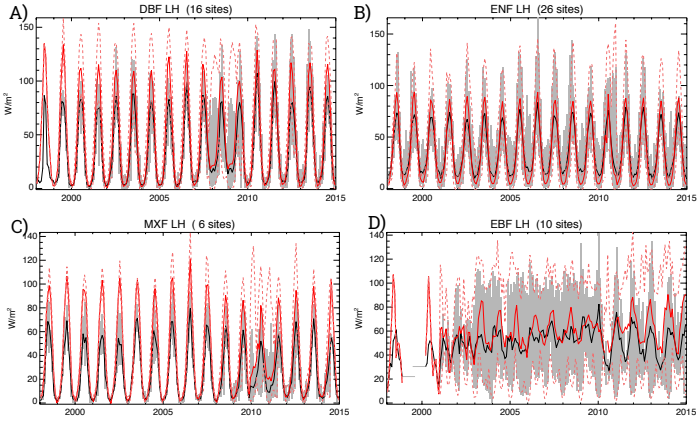

Fig. 10. FLUXNET2015 (black) and SiB4 (red) monthly mean LH at forest sites. A) Deciduous Broadleaf Forest (DBF), B) Evergreen Needleleaf Forest (ENF), C) Mixed Forest (MXF), and D) Evergreen Broadleaf Forest (EBF).

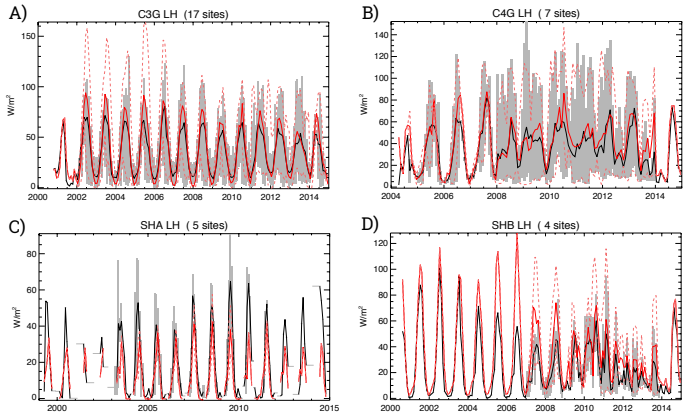

Fig. 11. FLUXNET2015 (black) and SiB4 (red) monthly mean LH at grassland (top) and shrub (bottom) sites. A) C3 non-arctic grassland (C3G), B) C4 grassland (C4G), C) arctic shrub (SHA), and D) non-arctic shrub (SHB).

Latent heat fluxes for grasslands and shrubs are shown in Figure 11. SiB4 overestimates the amplitude of the seasonal cycle in LH for C3 grasslands by 2-14 $W\,m^{-2}$ nearly every year. In contrast, the predicted LH for C4 grasslands more-closely matches the observations, with differences $<5\,W\,m^{-2}$. For arctic shrubs, SiB4 underestimates the summer latent heat

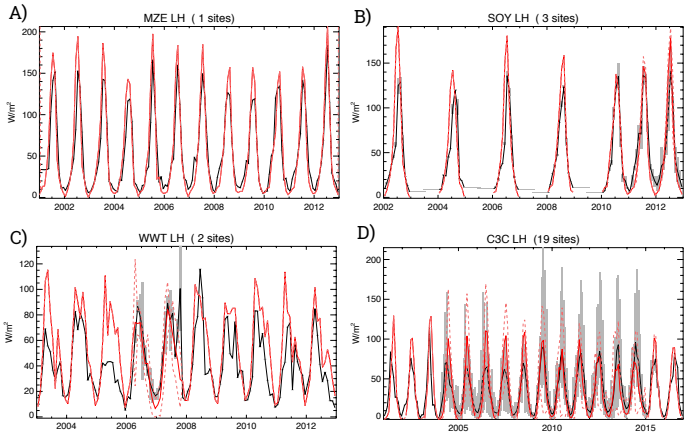

Fig. 12. FLUXNET2015 (black) and SiB4 (red) monthly mean LH at crop sites. A) Maize (MZE), B) Soybean (SOY), C) Winter Wheat (WWT), and D) Generic C3 Crops (C3C).

flux; however, for non-arctic shrubs SiB4 overestimates LH for some years, particularly when only one site is available.

Finally, crop latent heat fluxes are shown in Figure 12. At the MZE, SOY, and WWT sites, SiB4 overestimates the maximum latent heat flux during the summer by up to 15%. For non-specific C3 croplands, SiB4 overestimates LH from 2004-2009 by nearly 40%, but then underestimates LH by $\sim$10% in 2013 and 2014. These differences in the mean LH occur during times when there are large observed differences across the sites, thus SiB4 stays within the observed range of LH and near the middle of the distribution in most months.

5) Sensible Heat Flux: Sensible heat fluxes (SH) are shown in Figures 13-15. For forests (Figure 13), the flux magnitudes between observed and modeled are similar, including seasonal minimum, mean, and maximum vales. At the ENF and MXF sites, SiB4 seasonal cycle timing matches the observations; however, for DBF sites SiB4 shifts the timing of the fluxes by $\sim$1 month later than observed. For tropical forests, SiB4 underestimates the seasonal cycle from 2003-2008, when it then predicts SH with differences $<5\,W\,m^{-2}$ through 2014.

For grasslands and shrubs (Figure 14), SiB4 matches the observations within the range across sites; however, for C4 grasslands and non-arctic shrubs SiB4 systematically underestimates the SH by $\sim$10 $W\,m^{-2}$. This systematic underestimation accompanies the overestimation seen in LH, which could indicate that the SiB4 vegetation is stressed.

Finally, SH for crops is shown in Figure 15. The sensible heat flux for MZE and C3C match up both in timing and magnitude. Larger discrepancies occur for SOY and WWT, with differences up to 20 $W\,m^{-2}$, and these occur in 2002-2006 for SOY and in 2009-2010 for WWT. It is unclear as to what is causing these differences, but we hypothesize it could be related to irrigation and soil moisture availability.

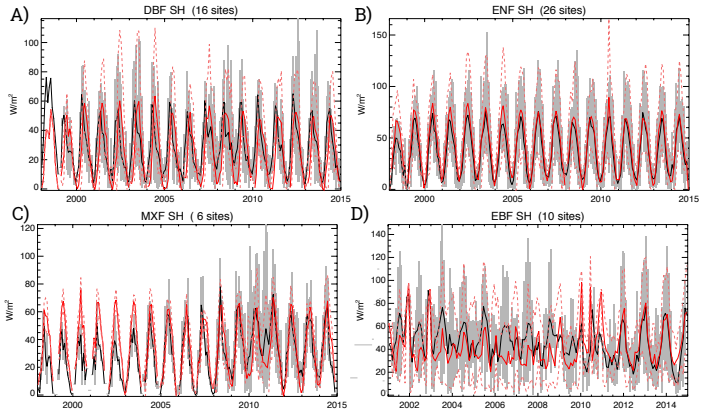

Fig. 13. FLUXNET2015 (black) and SiB4 (red) monthly mean SH at forest sites. A) Deciduous Broadleaf Forest (DBF), B) Evergreen Needleleaf Forest (ENF), C) Mixed Forests (MXF), and D) Evergreen Broadleaf Forest (EBF).

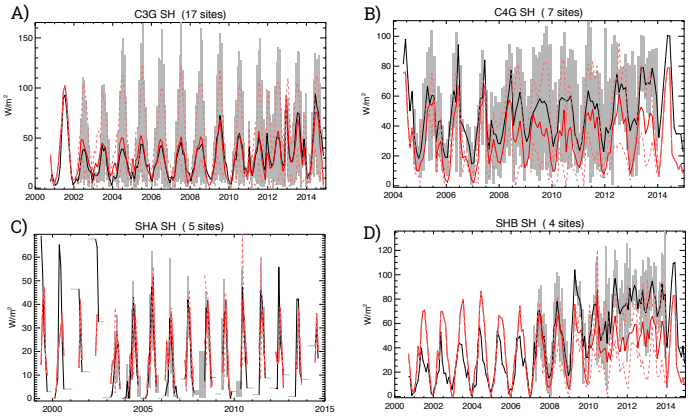

Fig. 14. FLUXNET2015 (black) and SiB4 (red) monthly mean SH at grassland (top) and shrub (bottom) sites. A) C3 non-arctic grassland (C3G), B) C4 grassland (C4G), C) arctic shrub (SHA), and D) non-arctic shrub (SHB).

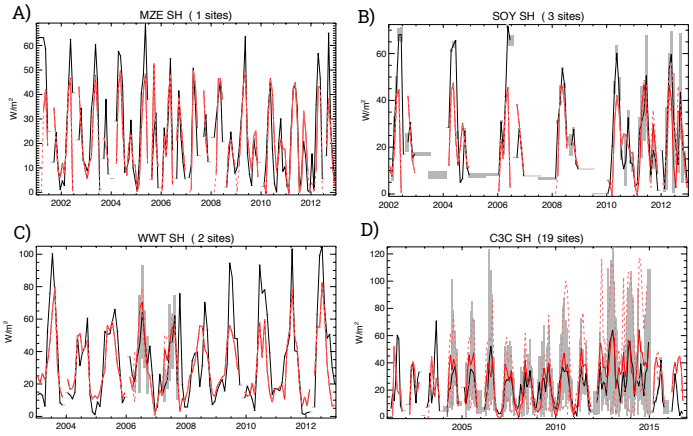

Fig. 15. FLUXNET2015 (black) and SiB4 (red) monthly mean SH at crop sites. A) Maize (MZE), B) Soybean (SOY), C) Winter Wheat (WWT), and D) Generic C3 Crops (C3C).

B. Global Evaluation

We evaluated SiB4 GPP against two different global products at 0.5-degree resolution for the time period from 2000 to 2011. The first, by Jung et al. [2011] (hereafter referred to as J11), uses machine learning to upscale Fluxnet observations. The second, by Zhang et al. [2017] (hereafter referred to as Z17), uses satellite data from MODIS and climate data from the NCEP Reanalysis II in an improved light use efficiency theory. For all three datasets, we compared the mean annual GPP ($\mathrm{g\,C\,m^{-2}\,yr^{-1}}$) (Figure 16).

Maps of the global mean GPP are shown in Figure 16A. Tropical forests are immediately evident in all three products, and southeast Asia has regions with high GPP of $\sim$3000 $\mathrm{g\,C\,m^{-2}\,s^{-1}}$. The southeast US has moderately high GPP of $\sim$1800-2000, with a sharp gradient in moving west as forests transition to grasslands. Europe also has moderate annual GPP and is more similar between maps, with $\sim$1500 $\mathrm{g\,C\,m^{-2}\,s^{-1}}$ annual mean uptake. Finally, boreal forests in Russian and Siberia are clearly evident in all three maps, with annual GPP of $\sim$900 $\mathrm{g\,C\,m^{-2}\,s^{-1}}$.

While the large-scale patterns appear similar between all three, differences can clearly be seen in Figure 16B. These figures show that SiB4 has the highest GPP over tropical forests by $\sim$100-500 $\mathrm{g\,C\,m^{-2}\,s^{-1}}$ over the other two products. While SiB4 has the highest GPP over Amazonia and equatorial Africa, differences of the same magnitude are evident between the two products in smaller regions of these areas. Thus in general, SiB4 is similar to J11 in the tropics and has larger differences from J11 in higher latitudes, where SiB4 has lower uptake in boreal forests. In contrast, SiB4 differences from Z17 are greater in the tropics, while the fluxes are within $\sim$100 $\mathrm{g\,C\,m^{-2}\,s^{-1}}$ in higher latitudes in both hemispheres.

Persistent smaller-scale differences between the products can been seen in the latitudinal distribution of GPP shown in Figure 16C. The figure shows that in the tropics, J11 has the highest GPP at the equator with relatively symmetrical decreasing GPP with increasing latitude, whereas Z17 shifts the highest GPP uptake southward and has a broader region of high GPP. SiB4 tropical GPP is between these two maps, with a peak near the equator similar to J11 but with a magnitude similar to Z17. Moving to higher latitudes, SiB4 and J11 have similar latitudinal gradients, while Z17 extends higher GPP to slightly higher latitudes. Around 50° N SiB4 shifts from matching J11 to more closely matching Z17, with lower GPP in boreal forests than J11. In the Southern Hemisphere, SiB4 and Z17 have a smoother gradient of decreasing GPP with increasing latitude, while J11 has latitude bands with locally rapid increases and decreases in GPP.

Finally, global annual mean GPP for all three products can be seen in Figure 16D. All three products are within 10 Pg C from 2000 until 2012, when the SiB4 and Z17 annual totals diverge. Starting in 2000, SiB4 and J11 are more similar in magnitude and lower than Z17. They also both show the lowest annual GPP in 2002 before exhibiting similar trends of increasing global annual mean GPP through 2011. Although

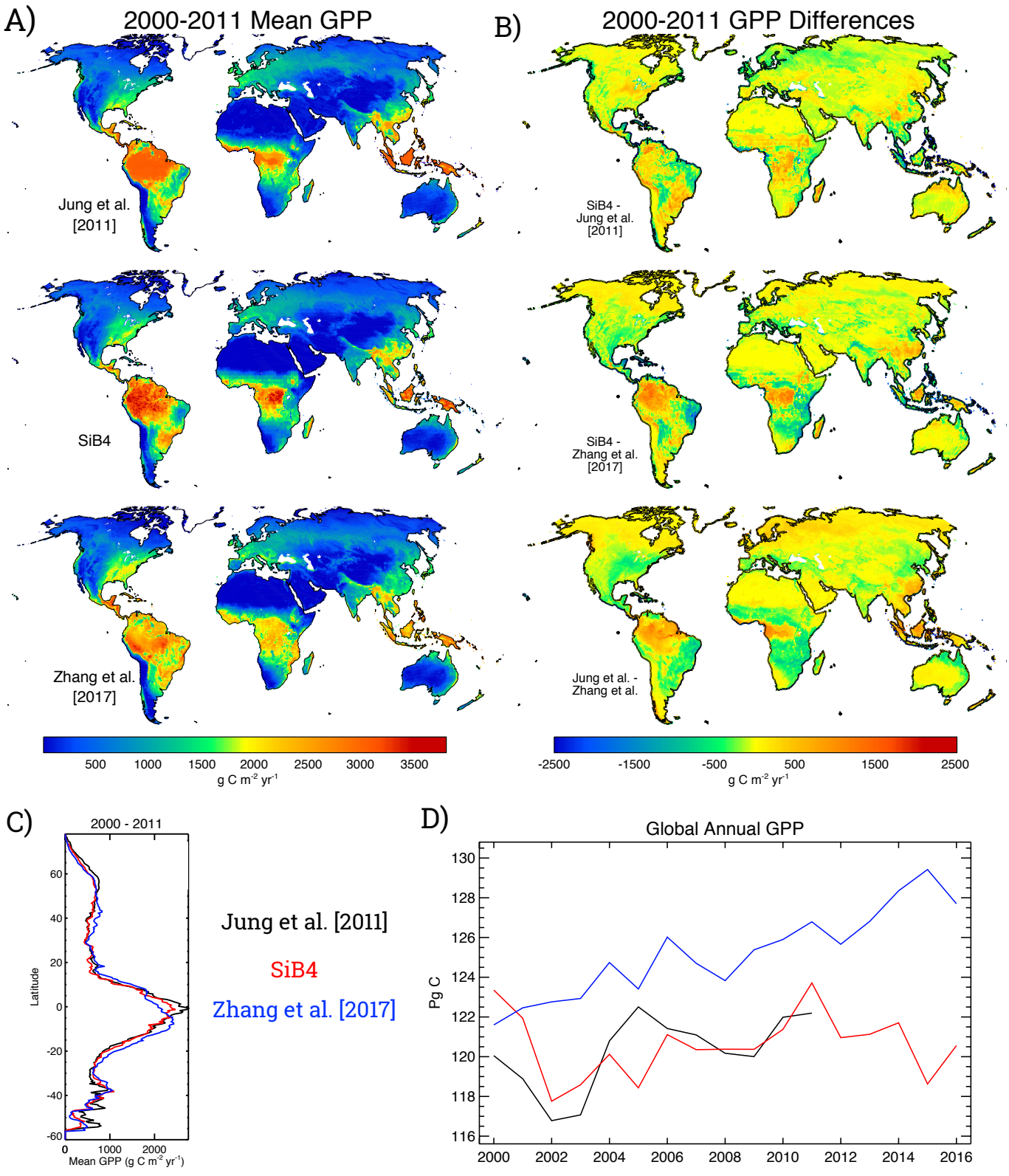

Fig. 16. Mean Annual GPP for 2000-2011. A) Maps from Jung et al. [2011] (top), SiB4 (middle), and Zhang et al. [2017] (bottom). B) Differences between SiB4 and Jung et al. [2011] (top), SiB4 and Zhang et al. [2017] (middle), and Zhang et al. [2017] and Jung et al. [2011] (bottom). C) GPP by latitude, with Jung et al. [2011] in black, SiB4 in red, and Zhang et al. [2017] in blue. D) Interanual variability of annual global total GPP.

Z17 has a few minor dips in GPP, in general it shows increasing mean annual GPP with time.

The divergence in GPP between SiB4 and Z17 could be due to several different mechanisms. First, since biomass burning begins in SiB4 in 2003, this could be due to an accumulation of removed carbon decreasing the GPP in SiB4. There have also been more notable droughts recently, particularly in North America and Europe, and the lower GPP in SiB4 could be reflective of this. Finally, SiB4 has steady state carbon pools other than biomass burning, and thus does not include mechanisms for increasing GPP on annual timescales that may be contributing to increasing GPP seen in Z17, such as nitrogen fertilization and boreal warming.

II. Leaf Area Index

We evaluated SiB4 leaf area index (LAI) globally against satellite data from the MODerate Imaging Spectroradiometer (MODIS) available from 2000-2016. At the selected Fluxnet sites, we used the pre-processed MODIS LAI available from the MODIS Land Product Subsets Project (ORNL DAAC, 2008a, 2008b). These MODIS LAI data are 8-day composites that have been specifically subset for predefined ares of $\sim$8 x 8 km centered on towers, and we compared average LAI from Terra and Aqua to SiB4 output on the same days as the satellite measurements. The sites where the subset product is available are notated in Table I.

For global evaluation, we used the MOD15A2 and MYD15A2 products (Myneni et al. [2015]). We combined the 8-day 500 m data into monthly 0.5-degree bins, averaging the Terra and Aqua products. We compared the June-July-August (JJA) mean over the 15 years against the corresponding mean SiB4 LAI.

A. Site Comparisons

LAI for forest, grassland, and shrub sites are shown in Figures 17 and 18. SiB4 has higher mean LAI than MODIS for forest PFTs (Figure 17). Although the mean SiB4 LAI is within the range seen by MODIS across sites, SiB4 has higher maximum LAI across the sites by 0.5-1.5 $m^2\,m^{-2}$. For DBF, SiB4 has a delayed leaf onset and senescence compared to MODIS; however, the timing of green-up at mixed forest sites matches that seen in MODIS. For ENF, SiB4 has substantially larger LAI than MODIS ($>$1.5 $m^2\,m^{-2}$), which is somewhat surprising given that SiB4 had lower GPP over regions characterized by this vegetation cover. Since this PFT keeps the needles yearround, while there is some flushing, it seems unlikely that forest LAI drops as much as that seen by MODIS, indicating that other factors such as high solar zenith angles or albedo are playing a role in the seasonality in the MODIS observations. For EBF, SiB4 has higher LAI than MODIS by $\sim$0.6 $m^2\,m^{-2}$ and leads the seasonality seen by MODIS by $\sim$1 month. Despite the slight high bias in LAI, the amplitude of the seasonality in the tropics is similar between the two products and remains relatively constant throughout the entire time period.

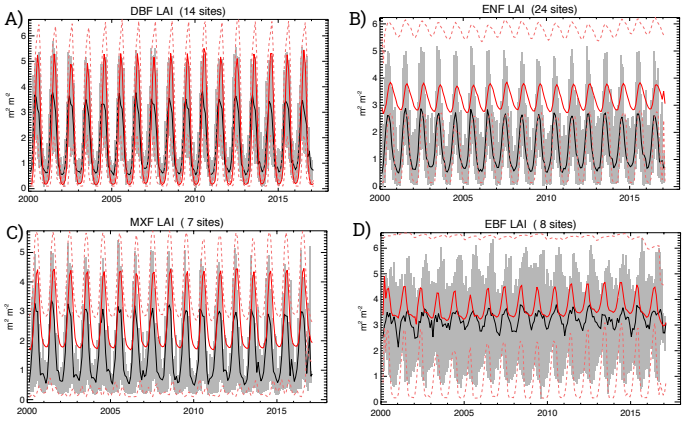

Fig. 17. MODIS (black) and SiB4 (red) LAI at forest sites. A) Deciduous Broadleaf Forest (DBF), B) Evergreen Needleleaf Forest (ENF), C) Mixed Forests (MXF), and D) Evergreen Broadleaf Forest (EBF).

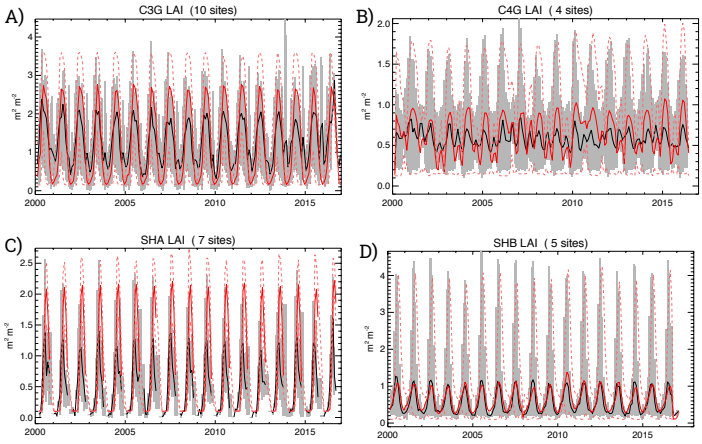

Fig. 18. MODIS (black) and SiB4 (red) monthly mean LAI at grassland (top) and shrub (bottom) sites. A) C3 non-arctic grassland (C3G), B) C4 grassland (C4G), C) arctic shrub (SHA), and D) non-arctic shrub (SHB).

LAI comparisons for grassland and shrub sites are shown in Figure 18. The timing of green-up and senescence is very similar for grasslands and shrubs. For grasslands, the mean SiB4 LAI remains within 0.3 $m^2\,m^{-2}$ of the mean MODIS LAI, which indicates differences are generally $<$ 15%; however, SiB4 overestimates the amplitude of the seasonal cycle at the C3 sites compared to MODIS. For arctic shrubs, the LAI is highly seasonal, and SiB4 estimates are on the high side of the range seen by MODIS. In non-arctic shrubs, mean SiB4 LAI is very similar to MODIS, with differences $<$0.2 $m^2\,m^{-2}$ over the entire time period. SiB4 also sees a similar spread of LAI across the sites as MODIS, as seen in the maximum LAI values across sites; however, the maximum LAI in SiB4 occurs slightly later than seen by MODIS. Although the MODIS to SiB4 LAI comparisons have substantial differences for many PFTs and have higher uncertainty than that seen for carbon and energy fluxes, this evaluation illustrates the high spatial

and temporal variability in LAI and indicates that SiB4 LAI predictions generally fall within this range of variability seen by satellite.

B. Global Evaluation

Global maps of mean JJA LAI for 2000-2014 from both MODIS and SiB4 are shown in Figure 19. The spatial distribution for both products is similar, with higher LAI in productive regions with high GPP and low LAI over drier regions and in higher latitudes. Both products have LAI values of 6-7 $m^2\ m^{-2}$ in the tropical forests. In Africa, the equatorial tropical forest is surrounded both north and south by gradients in vegetation coverage down to negligable LAI in the Sahara and southern Africa. In higher Northern latitudes, European countries and the U.S.A. have regions of forest and summer crops that form localized regions of higher LAIin JJA, and the boreal forests across North America and Asia create a band of high LAI across both continents.

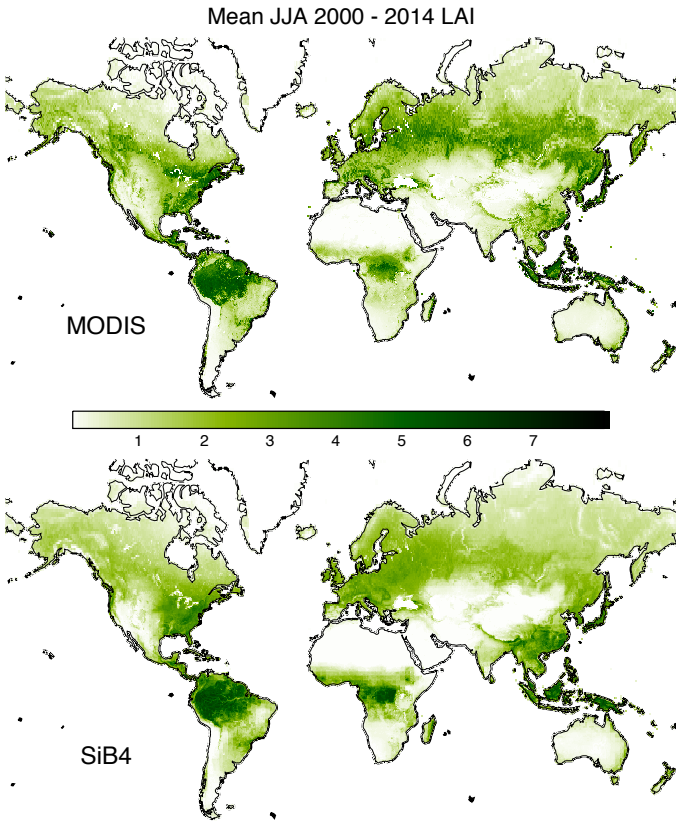

Fig. 19. Mean JJA LAI for 2000-2014 for MODIS (top) and SiB4 (bottom).

To highlight the differences by latitude, Figure 20 shows the mean LAI by latitude. This pattern supports the results from the site comparisons: SiB4 has higher mean LAI than MODIS in the tropics and lower LAI in higher latitudes. Surprisingly, SiB4 has lower LAI in both northern and southern temperate latitudes, which may suggest that the higher LAI seen at the deciduous forests and C3 grassland sites is not representative across larger regions or there are regions with high LAI seen in MODIS but not predicted by SiB4.

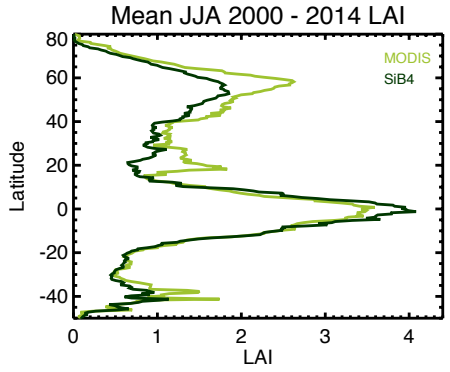

Fig. 20. Mean JJA LAI by latitude (MODIS, light green; SiB4, dark green).

To investigate the spatial patterns of these differences, Figure 21 shows maps of the differences. The higher tropical LAI in SiB4 is predominantly due to higher SiB4 LAI in equatorial Africa. Gradients of LAI differences can be seen in several continents. In Africa, SiB4 has higher LAI than MODIS over the coastal regions dominanted by tropical forest, while inland SiB4 has lower LAI in the sahel and grasslands. South America shows bands of higher SiB4 LAI in the Amazon, switching to lower LAI in SiB4 in central regions during the transition between tropical forest to grassland, ending with slightly higher LAI in the southern grasslands and savannas. In the Northern Hemisphere, SiB4 has higher LAI in central US and Europe, likely due to the impact of crops. In higher latitudes, SiB4 has less of an increase in LAI for boreal forests than MODIS, which could be contributing to the lower GPP predicted by SiB4 over this region. While regions exist with differences up to 3 $m^2\ m^{-2}$, in general the patterns of LAI for MODIS and SiB4 are similar with differences $<=1\ m^2\ m^{-2}$.

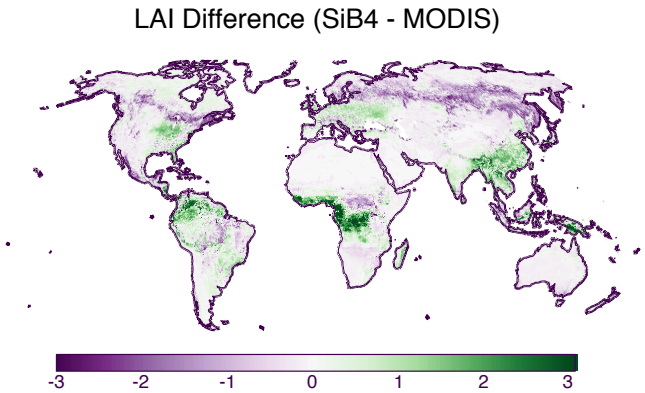

Fig. 21. Mean JJA LAI differences between SiB4 and MODIS.

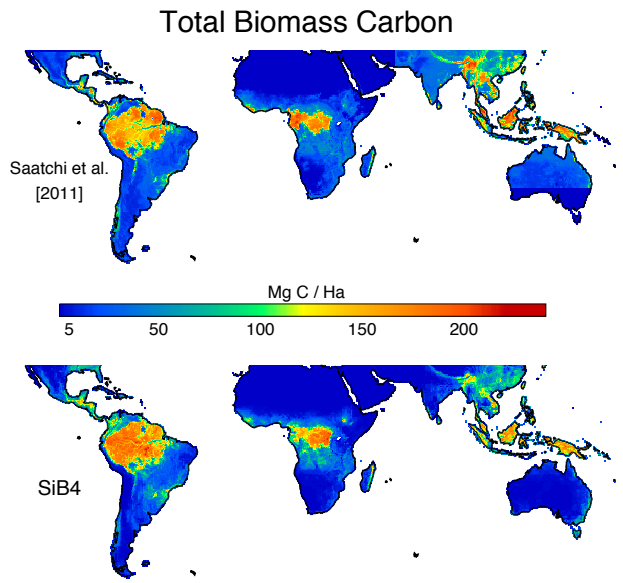

Fig. 22. Total carbon biomass from Saatchi et al. [2011] (top) and SiB4 (bottom).

III. Biomass

We compared SiB4 biomass against remotely-sensed biomass by Saatchi et al. [2011] (Figure 22). The biomass maps show similar patterns, with regions of high biomass in tropical forests and low biomass outside of the tropical forests. Small-scale changes in biomass can be seen in both products, such as lower biomass regions surrounding roads and rivers and patches of forest clearing. The biomass rapidly decreases outside the tropical forests on both continents as the vegetation rapidly transitions through savannas to grasslands.

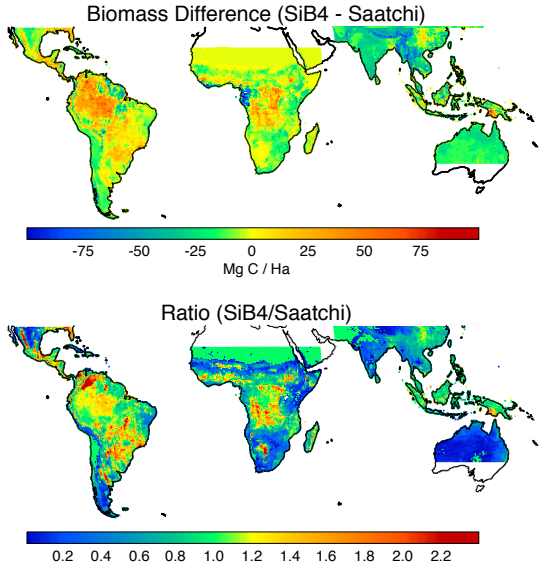

Fig. 23. Differences in biomass between SiB4 and Saatchi et al. [2011] (top) and the ratio between biomass estimates (bottom).

Looking at the differences between maps shown in Figure 23, SiB4 overestimates the biomass in much of the Amazon and in the regions of equatorial Africa, with differences of up to $100\,\mathrm{Mg\,C\,ha^{-2}}$. Along the coast of equatorial Africa, SiB4 underestimates the biomass by $\sim 75\,\mathrm{Mg\,C\,ha^{-2}}$. Comparing this against existing biomass, while many areas have ratios of the SiB4 to Saatchi et al. [2011] biomass ranging between 0.8 to 1.2, localized regions exist where the ratio is >2. Rather than broad regional differences between SiB4 and Saatchi et al. [2011] throughout Indonesia and southeastern Asia, areas of localized higher and lower biomass exist in these regions; and differences between Australian and Indian EBF regions are minimal ($<25\,\mathrm{Mg\,C\,ha^{-2}}$).

IV. Conclusions

This SiB4 output presents consistent predictions of carbon and energy fluxes, LAI, biomass, and other diagnostic variables. For all of these variables, SiB4 output falls within ranges of estimates from various different *in situ* and remotely sensed products for all vegetation types.

Acknowledgements

We thank the European Fluxnet community for making their fluxes publicly available, and in particular we thank site PIs Gerard Kiely (IE-Dri), Dario Papale (IT-Ro3), Joao Santos Pereira (PT-Mi1), Bart Kruijt (NL-Lut, NL-Lan and NL-Mol), Thomas Friborg (DK-Ris), Albert Olioso (FR-Avi), Mike Jones and Bruce Osborne (IE-Ca1), and Keith Goulding (UK-Her).

C3 Grassland (C3G)	
Site	**DOI**
AT-Neu*	https://doi.org/10.18140/FLX/1440121
AU-Rig	https://doi.org/10.18140/FLX/1440202
CH-Cha*	https://doi.org/10.18140/FLX/1440131
CH-Fru*	https://doi.org/10.18140/FLX/1440133
CH-Oe1*	https://doi.org/10.18140/FLX/1440135
CN-Du2	https://doi.org/10.18140/FLX/1440140
CN-Sw2	https://doi.org/10.18140/FLX/1440212
CZ-BK2*	https://doi.org/10.18140/FLX/1440144
DE-Gri*	https://doi.org/10.18140/FLX/1440147
DK-Eng	https://doi.org/10.18140/FLX/1440153
IE-Dri	http://www.europe-fluxdata.eu/home/
IT-MBo*	https://doi.org/10.18140/FLX/1440170
IT-Noe	https://doi.org/10.18140/FLX/1440171
IT-Ro3	http://www.europe-fluxdata.eu/home/
IT-Tor	https://doi.org/10.18140/FLX/1440237
NL-Hor*	https://doi.org/10.18140/FLX/1440177
RU-Ha1*	https://doi.org/10.18140/FLX/1440184
US-Goo	https://doi.org/10.18140/FLX/1440070
US-Var*	https://doi.org/10.18140/FLX/1440094

C4 Grassland (C4G)	
AU-DaP*	https://doi.org/10.18140/FLX/1440123
AU-Stp*	https://doi.org/10.18140/FLX/1440204
PA-SPs	https://doi.org/10.18140/FLX/1440179
US-ARc	https://doi.org/10.18140/FLX/1440065
SD-Dem*	https://doi.org/10.18140/FLX/1440186
US-AR1	https://doi.org/10.18140/FLX/1440103
US-AR2	https://doi.org/10.18140/FLX/1440104
US-IB2	https://doi.org/10.18140/FLX/1440072
US-Wkg*	https://doi.org/10.18140/FLX/1440096

Deciduous Broadleaf Forest (DBF)	
CA-Oas*	https://doi.org/10.18140/FLX/1440043
CA-TPD	https://doi.org/10.18140/FLX/1440112
CN-Din	https://doi.org/10.18140/FLX/1440139
DE-Hai*	https://doi.org/10.18140/FLX/1440148
DE-Lnf*	https://doi.org/10.18140/FLX/1440150
DE-Zrk	https://doi.org/10.18140/FLX/1440221
DK-Sor*	https://doi.org/10.18140/FLX/1440155
FR-Fon*	https://doi.org/10.18140/FLX/1440161
IT-CA1	https://doi.org/10.18140/FLX/1440230
IT-Col*	https://doi.org/10.18140/FLX/1440167
IT-Isp	https://doi.org/10.18140/FLX/1440234
IT-PT1	https://doi.org/10.18140/FLX/1440172
IT-Ro1*	https://doi.org/10.18140/FLX/1440174
IT-Ro2*	https://doi.org/10.18140/FLX/1440175
JP-MBF	https://doi.org/10.18140/FLX/1440238
PA-SPn	https://doi.org/10.18140/FLX/1440180
US-Ha1*	https://doi.org/10.18140/FLX/1440071
US-MMS*	https://doi.org/10.18140/FLX/1440083
US-Oho*	https://doi.org/10.18140/FLX/1440088
US-Syv*	https://doi.org/10.18140/FLX/1440091
US-UMB*	https://doi.org/10.18140/FLX/1440093
US-WCr*	https://doi.org/10.18140/FLX/1440095
US-Wi3	https://doi.org/10.18140/FLX/1440057
ZM-Mon	https://doi.org/10.18140/FLX/1440189

Evergreen Broadleaf Forest (EBF)	
AU-Cum	https://doi.org/10.18140/FLX/1440196
AU-Rob	https://doi.org/10.18140/FLX/1440203
AU-Tum*	https://doi.org/10.18140/FLX/1440126
AU-Whr	https://doi.org/10.18140/FLX/1440206
AU-Wom	https://doi.org/10.18140/FLX/1440207
BR-Sa1*	https://doi.org/10.18140/FLX/1440032
BR-Sa3*	https://doi.org/10.18140/FLX/1440033
FR-Pue*	https://doi.org/10.18140/FLX/1440164
GF-Guy*	https://doi.org/10.18140/FLX/1440165
GH-Ank*	https://doi.org/10.18140/FLX/1440229
IT-Cpz*	https://doi.org/10.18140/FLX/1440168
MY-PSO	https://doi.org/10.18140/FLX/1440240
PT-Mi1*	http://www.europe-fluxdata.eu/home/

Continued on next column

Continued from previous column

Evergreen Needleleaf Forest (ENF)	
Site	**DOI**
AR-Vir	https://doi.org/10.18140/FLX/1440192
CA-Man*	https://doi.org/10.18140/FLX/1440035
CA-NS1	https://doi.org/10.18140/FLX/1440036
CA-NS3*	https://doi.org/10.18140/FLX/1440038
CA-Obs*	https://doi.org/10.18140/FLX/1440044
CA-Qfo*	https://doi.org/10.18140/FLX/1440045
CA-TP4*	https://doi.org/10.18140/FLX/1440053
CH-Dav*	https://doi.org/10.18140/FLX/1440132
CN-Qia	https://doi.org/10.18140/FLX/1440141
CZ-BK1*	https://doi.org/10.18140/FLX/1440143
DE-Lkb	https://doi.org/10.18140/FLX/1440214
DE-Obe*	https://doi.org/10.18140/FLX/1440151
DE-Tha*	https://doi.org/10.18140/FLX/1440152
FI-Hyy*	https://doi.org/10.18140/FLX/1440158
FI-Let	https://doi.org/10.18140/FLX/1440227
FI-Sod*	https://doi.org/10.18140/FLX/1440160
IT-Lav*	https://doi.org/10.18140/FLX/1440169
IT-Ren*	https://doi.org/10.18140/FLX/1440173
IT-SRo*	https://doi.org/10.18140/FLX/1440176
IT-SR2	https://doi.org/10.18140/FLX/1440236
NL-Loo*	https://doi.org/10.18140/FLX/1440178
RU-Fyo*	https://doi.org/10.18140/FLX/1440183
US-Blo*	https://doi.org/10.18140/FLX/1440068
US-GBT*	https://doi.org/10.18140/FLX/1440118
US-GLE*	https://doi.org/10.18140/FLX/1440069
US-Ho1*	https://doi.org/10.18140/FLX/1669675
US-KS1	https://doi.org/10.18140/FLX/1440074
US-Me2*	https://doi.org/10.18140/FLX/1440079
US-NR1*	https://doi.org/10.18140/FLX/1440087
US-Prr*	https://doi.org/10.18140/FLX/1440113
US-Wi4*	https://doi.org/10.18140/FLX/1440058

Mixed Forest (MXF)	
AR-SLu	https://doi.org/10.18140/FLX/1440191
BE-Bra*	https://doi.org/10.18140/FLX/1440128
BE-Vie*	https://doi.org/10.18140/FLX/1440130
CA-Gro*	https://doi.org/10.18140/FLX/1440034
CH-Lae*	https://doi.org/10.18140/FLX/1440134
CN-Cha*	https://doi.org/10.18140/FLX/1440137
JP-SMF	https://doi.org/10.18140/FLX/1440239
US-PFa*	https://doi.org/10.18140/FLX/1440089
US-SRC*	https://doi.org/10.18140/FLX/1440098

Shrub (Arctic) (SHA)	
FI-Lom*	https://doi.org/10.18140/FLX/1440228
RU-Che*	https://doi.org/10.18140/FLX/1440181
RU-Cok*	https://doi.org/10.18140/FLX/1440182
SE-St1*	https://doi.org/10.18140/FLX/1440187
US-Atq*	https://doi.org/10.18140/FLX/1440067
US-ICs*	https://doi.org/10.18140/FLX/1669678
US-Ivo*	https://doi.org/10.18140/FLX/1440073

Shrub (Non-Arctic) (SHB)	
AU-ASM*	https://doi.org/10.18140/FLX/1440194
DE-Spw	https://doi.org/10.18140/FLX/1440220
ES-Amo*	https://doi.org/10.18140/FLX/1440156
ES-LgS*	https://doi.org/10.18140/FLX/1440225
US-Los*	https://doi.org/10.18140/FLX/1440076
US-Whs*	https://doi.org/10.18140/FLX/1440097

Maize (MZE)	
US-Ne1	https://doi.org/10.18140/FLX/1440084

Soybean (SOY)	
US-CRT	https://doi.org/10.18140/FLX/1440117
US-Ne2	https://doi.org/10.18140/FLX/1440085
US-Ne3	https://doi.org/10.18140/FLX/1440086

Continued on next column

Continued from previous column

Winter Wheat (WWT)	
Site	**DOI**
NL-Lut*	http://www.europe-fluxdata.eu/home/
US-ARM*	https://doi.org/10.18140/FLX/1440066
C3 Crops (C3C)	
AU-Ync	https://doi.org/10.18140/FLX/1440208
BE-Lon*	https://doi.org/10.18140/FLX/1440129
CH-Oe2*	https://doi.org/10.18140/FLX/1440136
CN-Cng*	https://doi.org/10.18140/FLX/1440209
DE-Geb*	https://doi.org/10.18140/FLX/1440146
DE-Kli*	https://doi.org/10.18140/FLX/1440149
DE-RuS	https://doi.org/10.18140/FLX/1440216
DE-Seh	https://doi.org/10.18140/FLX/1440217
DK-Fou*	https://doi.org/10.18140/FLX/1440154
DK-Ris*	http://www.europe-fluxdata.eu/home/
FI-Jok	https://doi.org/10.18140/FLX/1440159
FR-Avi*	http://www.europe-fluxdata.eu/home/
IE-Ca1	http://www.europe-fluxdata.eu/home/
IT-Cas	https://doi.org/10.18140/FLX/1669645
NL-Lan	http://www.europe-fluxdata.eu/home/
NL-Mol*	http://www.europe-fluxdata.eu/home/
UK-Her*	http://www.europe-fluxdata.eu/home/
US-Lin	https://doi.org/10.18140/FLX/1440107
US-Tw3	https://doi.org/10.18140/FLX/1440110
US-Twt	https://doi.org/10.18140/FLX/1440106

Sites with * indicates MODIS LAI is available.

Concluded

TABLE I
FLUXNET SITE IDS AND DOIS.

REFERENCES

[1] Barr, A.G., Richardson, A.D., Hollinger, D.Y., Papale, D., Arain, M.A., Black, T.A., ..., & Schaeffer, K. (2013). Use of change-point defection for friction-velocity threshold evaluation in eddy-covariance studies. *Agric. For. Meteorol.*, **171-172**, 31-45, https://doi.org/10.1016/j.agformet.2012.11.023.

[2] Commane, R., Lindaas, J., Benmergui, J., Luus, K.A., Chang, R.Y.-W., Baube, B.C., ..., & Wofsy, S.C. (2017). Carbon dioxide sources from Alaska driven by increasing early winter respiration from Arctic tundra. *Proc. Natl. Acad. Sci. U.S.A.*, **114**(21), 5361-5366, https://doi.org/10.1073/pnas.1618567114.

[3] Jung, M., Reichstein, M., Margolis, H.A., Cescatti, A., Richardson, A.D., Arain, M.A., ..., & Williams, C. (2011). Global patterns of land-atmosphere fluxes of carbon dioxide, latent heat, and sensible heat derived from eddy covariance, satellite, and meteorological observations. *J. Geophys. Res.*, **116**(G00J07), https://doi.org/10.1029/2010JG001566.

[4] Lasslop, G., Reichstein, M., Papale, D., Richardson, A.D., Arneth, A., Barr, A., Stoy, P., & Wohlfahrt, G. (2010). Separation of net ecosystem exchange into assimilation and respiration using a light response curve approach: crucial issues and global evaluation. *Glob. Change Biol.*, **16**, 187-208, https://doi.org/10.1111/j.1365-2486.2009.02041.x.

[5] Myneni, R., Knyazikhin, Y., & Park, T. (2015). MOD15A2H MODIS Leaf Area Index/FPAR 8-Day L4 Global 500m SIN Grid V006. NASA EOSDIS Land Processes DAAC. http://doi.org/10.5067/MODIS/MOD15A2H.006; http://doi.org/10.5067/MODIS/MYD15A2H.006.

[6] ORNL DAAC (2008a). *MODIS collection 5 land products global subsetting and visualization tool.* Oak Ridge, Tennessee, USA: ORNL DAAC. Accessed August 2016. Subsets obtained for MOD15A2 product at various sites in spatial range: N=72.37N, S=35S, E=148.55E, W=157.40W, time period: 2002-02-18 to 2014-12-31, and subset size: 0.25x0.25 km, https://doi.org/10.334/ORNLDAAC/1241.

[7] ORNL DAAC (2008b). *MODIS collection 5 land products global subsetting and visualization tool.* Oak Ridge, Tennessee, USA: ORNL DAAC. Accessed August 2016. Subsets obtained for MYD15A2 product at various sites in spatial range: N=72.37N, S=35S, E=148.55E, W=157.40W, time period: 2002-02-18 to 2014-12-31, and subset size: 0.25x0.25 km, https://doi.org/10.334/ORNLDAAC/1241.

[8] Papale, D.M., Reichstein, M., Aubinet, M., Canfor, E., Bernhofer, C., Longdoz, B., ..., & Yakir, D. (2006). Towards a standardized processing of Net Ecosystem Exchange measured with eddy covariance technique: algorithms and uncertainty estimation. *Biogeosci.*, **3**, 571-583, https://doi.org/10.5194/bg-3-571-2006.

[9] Pastorello, G., Trotta, C., Canfora, E., Chu, H., Christianson, D., Cheah, Y.-W., ..., & Papale, D. (2020). The FLUXNET2015 dataset and the ONEFlux processing pipeline for eddy covariance data. *Sci. Data*, **7**(225), https://doi.org/10.1038/s41597-020-0534-3.

[10] Saatchi, S.S., Harris, N.L., Brown, S., Lefsky, M., Mitchard, E.T.A., Salas, W., ..., & Morel, A. (2011). Benchmark map of forest carbon stocks in tropical regions across three continents. *PNAS*, **108**(24), 9899-9904, https://doi.org/10.1073/pnas.1019576108.

[11] Zhang, Y. Xiao, X., Wu, X., Zhou, S., Zhang, G., Qin, Y., & Dong, J. (2017). A global moderate resolution dataset of gross primary production of vegetation for 2000-2016. *Sci. Data*, **4**(170165), https://doi.org/10.1038/sdata.2017.165.